Article ID：1007−7294(2025)06−0952−12

Fatigue Crack Growth Behavior of High-strength Steel for Ships

LEI Yin−hui[1], *WANG Ke*[1], *ZHANG Ruo−nan*[2,3], *LI Yong−zheng*[1], *QIN Chuang*[1], *WEI Peng−yu*[2,3]

(1. School of Naval Architecture and Ocean Engineering, Jiangsu University of Science and Technology, Zhenjiang 212003, China; 2. China Ship Scientific Research Center, Wuxi 214082, China; 3. Taihu Laboratory of Deepsea Technological Science, Wuxi 214082, China)

Abstract: As a typical steel, the fatigue of marine high-strength steels has been emphasized by scholars. In this paper, the fatigue performance and crack growth mechanism of a high-strength steel for ships are investigated by experimental methods. First, the fatigue threshold test and fatigue crack growth rate test of this high-strength steel under different stress ratios were carried out. The influence of stress ratio on the fatigue properties of this steel was analyzed. Secondly, scanning electron microscope was used to analyze the crack growth specimen section of this steel. The crack growth and failure mechanism of this steel were revealed. Finally, based on the above research results, the stress ratio effect of high-strength steel was investigated from the perspectives of crack closure and driving force. Considering the fatigue behavior in the near-threshold stage and the destabilization stage, a fatigue crack growth behavior prediction model of high-strength steel was established. The accuracy of the model was verified by test data. Moreover, the applicability of the modified model to various materials and its excellent predictive ability were verified through comparison with literature data and existing models.

Key words: high-strength steel; fatigue test; load ratio effect; dual-parameter-driving force; prediction model

CLC number：TG111.8 **Document code**：A **doi:** 10.3969/j.issn.1007−7294.2025.06.009

0 Introduction

With the development of modern engineering technology, the application of high-strength steel has become more and more widespread. Compared with ordinary steel, high-strength steel has significant advantages in terms of stress performance, processing and economic benefits. The increase in yield strength leads to an insignificant strain-strengthening effect during loading, which makes the fatigue performance of high-strength steel poor[1]. Fatigue damage is particularly prominent on ships, accounting for 80%−90% of its damage forms[2], causing great harm to the safe use of ships. Therefore, it is very important to conduct fatigue tests on high-strength steel and predict its fatigue performance in conjunction with the fracture of specimens.

The application of high-strength steel in the field of marine has been mainly reflected in the construction

Received date：2024−12−17

Foundation item：Supported by the National Natural Science Foundation of China (52071161) and the National Key Research and Development Program of China (2022YFB3404800)

Biography：LEI Yin-hui(1999–), female, master student; WANG Ke(1979–), female, professor, corresponding author, E-mail: ecsibelle@126.com.

of offshore platforms and ships. Liu et al[3] conducted an experimental study on the fatigue performance of DH36 steel, an offshore steel. It was found that an increase in the load ratio would lead to an elevation of the crack growth rate, while the fatigue threshold value would decrease accordingly. Wang et al[4] found the existence of significant differences in the crack growth behavior of EH36 under different load ratios. Not coincidentally, Zhong et al[5] also found that the load ratio has a remarkable effect on the fatigue behavior of EH36. Most scholars attribute this difference to crack closure during crack growth. Wang[6] investigated the crack closure behavior of 10Ni5CrMoV and found that the level of crack closure was enhanced with the increase of R, which led to the difference in crack growth behavior. However, on the other hand, some scholars believed that crack closure was not the main reason for the differences in crack growth behavior of steels. They began to ignore crack closure and turned to explain the fatigue behavior of steels from a completely new perspective. Kujawski[7] proposed the dual-parameter-driving force. He believed that both K_{max} and ΔK drive crack growth. Martelo et al[8] found that the dual-parameter-driving force could better explain the crack growth behavior of AISI 301 LN. The same conclusion was obtained by Wei[9]. Up to now, no scholar has given definite evidence to prove which of the two, crack closure theory or dual-parameter driving force, can better explain the crack growth behavior of steels, Some scholars have also modified the Paris model according to the loading conditions and material properties as a way to predict the crack growth behavior of metals[4,10−13]. The types and properties of steels used in different offshore structures vary greatly. As a typical steel for ships, the high-strength steel still has unclear fatigue crack growth and failure mechanism. So the study of the fatigue properties should not be delayed.

In this paper, the fatigue properties of a high-strength steel for ships were studied. Firstly, the basic mechanical properties tests were carried out at room temperature to obtain the fatigue thresholds of this steel. Secondly, the fatigue crack growth rate was obtained by the experiments under different stress ratios. Based on the crack closure and the driving force perspectives, the crack growth rate curves were processed to analyze the stress ratio effect. Scanning electron microscope (SEM) was used to analyze the crack growth and failure mechanism. A modified model was proposed considering the fatigue behavior in the near-threshold stage and unstable stage, based on the dual-parameter-driving model. The reliability of the modified model was verified by comparison with the experimental results. Moreover, by comparing with other prediction models, the universality and prediction ability of the modified model were verified.

1 Material and methods

The experimental material presented in this paper was a high-strength steel for ships. The yield strength of this steel was 653 MPa, while the tensile strength was 785 MPa. The chemical composition (wt.%) was 0.12 C, 0.33 Si, 0.37 Mn, 2.72 Ni, 1.05 Cr, 0.24 Mo, 0.08 V, 0.04 S, 0.08 P and balanced by Fe.

Based on ASTM E647, the fatigue threshold test and crack growth rate test were performed on Instron 8802 fatigue testing machine. Single-edge notch bend (SENB) specimen was used in all tests, with a width of 134.4 mm and a thickness of 15 mm. The detailed dimensions of the specimen were shown in Fig. 1.

Pre-cracking of the specimens was required before all tests started in order to eliminate the influence of notch effects and ensure that the crack tip was sufficiently sharp. The initial crack length was 6.8 mm. The fatigue threshold test was conducted by the descending load method, with the percentage of graded load reduction at 10%. During the load reduction, it was ensured that the crack growth at each load level should be 4~6 times the size of plastic region under previous load level. The crack growth rate test was performed at

five stress ratios, namely R = 0.1, 0.3, 0.4, 0.5 and 0.7. A constant amplitude load of 9000 N in sine wave with 10 Hz frequency were applied in the crack growth rate test. The load spectrum used in the fatigue test was shown in Fig. 2.

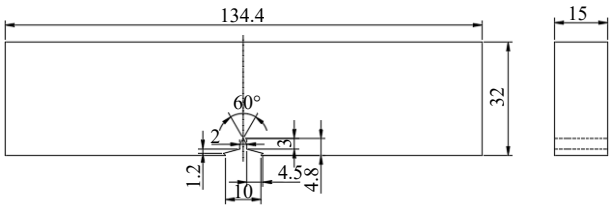

Fig.1 Size of SENB specimen (Unit: mm)

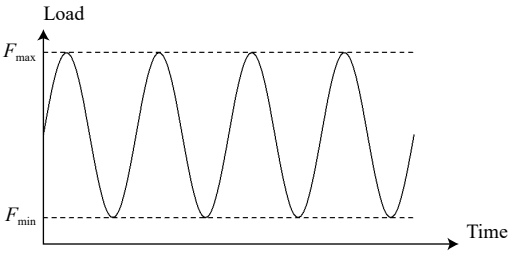

Fig.2 Load spectrum

2 Experimental results and discussion

2.1 Fatigue threshold test

The 5–10 sets of data with 1×10^{-7} mm/cycle $\leqslant \mathrm{d}a/\mathrm{d}N \leqslant 1\times10^{-6}$ mm/cycle in the threshold test results were selected. These data were fitted by Eq. (1) to obtain the relevant parameters[14]. The experimental and fitting results for R= 0.1, 0.3 and 0.5 are shown in Fig. 3.

$$\mathrm{d}a/\mathrm{d}N = A(\Delta K)^m \tag{1}$$

where A and m are fitting parameters.

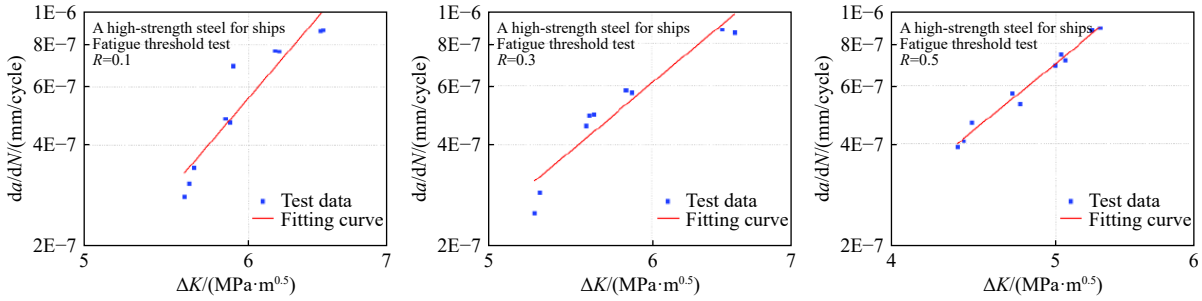

（a）R=0.1 （b）R=0.3 （c）R=0.5

Fig.3 Threshold test and fitting results of a high-strength steel at different stress ratios

Then the crack growth rate $\mathrm{d}a/\mathrm{d}N = 1\times10^{-7}$ mm/cycle was substituted into Eq. (1) to obtain the fatigue threshold value for different stress ratios[14]. According to the results of the threshold test, the fatigue thresholds of high-strength steel were 4.70, 4.10 and 3.05 MPa·m$^{0.5}$ for the stress ratios of 0.1, 0.3 and 0.5, respectively. The fatigue threshold of this high-strength steel decreased with the increase of R.

2.2 Fatigue crack growth rate test

The fatigue test results were processed using the seven-point incremental polynomial method to obtain the fatigue life $a-N$ curve. The slope of the $a-N$ curve was taken as the crack growth rate. The crack growth rate curve was derived by relating to the stress intensity factor range, which was calculated using Eq. (2) to Eq. (4).

$$\Delta K = \frac{\Delta F}{BW^{1/2}} g(\alpha) \tag{2}$$

$$g(\alpha) = \frac{6\alpha^{0.5}}{(1-2\alpha)\cdot(1-\alpha)^{1.5}} \cdot [1.99 - \alpha(1-\beta)\cdot(2.15-3.93\alpha+2.7\alpha^2)] \tag{3}$$

$$\alpha = \frac{a}{W} \tag{4}$$

where B is the thickness of the specimen (mm), W is the width of the specimen (mm), and ΔF is the load amplitude of the test (N).

The fatigue life curves of the high-strength steel, i.e. $a-N$ curves, were shown in Fig. 4. As could be seen from the figure, the initial length of cracks was the same for five load ratios (R = 0.1, 0.3, 0.4, 0.5, 0.7), which was about 6.8 mm. With the increase of the cycles, the crack length increased exponentially until the fatigue failure occurred. The crack lengths at the moment of fracture were 23.34, 21.89, 20.82, 19.83 and 16.06 mm for R = 0.1, 0.3, 0.4, 0.5 and 0.7, and the fatigue life were 184 041, 161 918, 146 996, 132 756 and 122 541 cycles, respectively. In other words, the fatigue crack growth life of this steel was reduced by 12.02%, 20.19%, 27.87% and 33.42% for stress ratios of 0.3, 0.4, 0.5 and 0.7, compared to R=0.1. The fatigue life became shorter with the increase of load ratio R. The increase in R led to a larger average load, which made the damage more severe. As a result, the fatigue life decreases.

Fig. 5 shows the experimental results of the fatigue crack growth rates of the high-strength steel under R = 0.1, 0.3, 0.4, 0.5 and 0.7. From the figure, it can be seen that the fatigue crack growth rate of this steel at different load ratios was significantly accelerated with the increase of load intensity factor range. When the maximum stress intensity factor reaches the fracture toughness of the material, the specimen fractures. The load ratio has a significant effect on the fatigue crack growth behavior. With the increase of stress ratio, the fatigue crack growth rate of this steel tends to increase. The Paris region is shortened, and the material enters the rapid growth phase at a lower stress intensity factor range.

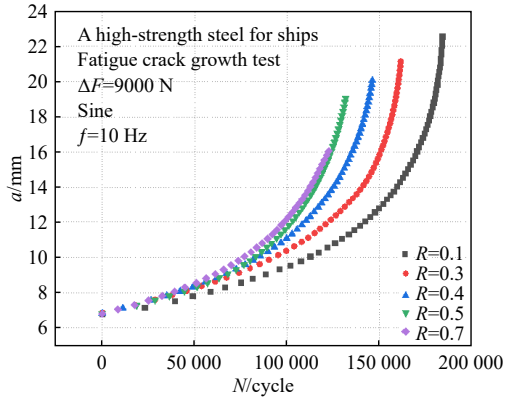

Fig.4 Fatigue crack growth life curves of high-strength steel under different load ratios

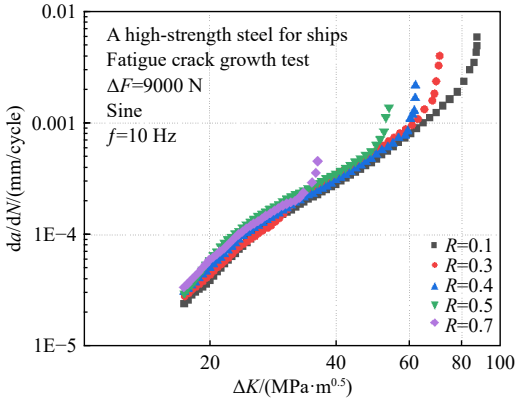

Fig.5 Fatigue crack growth rate curves of high-strength steel under different load ratios

At present, scholars mainly explain the effect of stress ratio on crack growth behavior of steels from two aspects, one is the crack closure[15−16] and the other is the driving force[8]. The crack closure suggests that there exists a critical load (also called open load) at the crack tip during crack growth. When the load is less than this critical load, the crack face is in a closed state. Only when the load is greater than this open load, the crack will develop. Therefore, it has been argued[16] that the real factor controlling crack growth is the effective stress intensity factor range, as shown in Eq. (5).

$$\Delta K_{\text{eff}} = K_{\max} - K_{\text{op}} \tag{5}$$

where ΔK_{eff} is the effective stress intensity factor range (MPa·m$^{0.5}$), K_{op} is the crack tension stress intensity factor (MPa·m$^{0.5}$).

When the load ratio is small, the stress level at the crack tip is low and the crack closure is severe. This will result in a smaller effective stress intensity factor, which in turn leads to a lesser crack growth rate.

With the increase of the load ratio, this phenomenon weakens or even disappears. Two well-known crack closure models have been used to explain the stress ratio effect on metals: the Elber's model[16] shown as Eq. (6), and the Schijve's model[17] shown as Eq. (7).

$$K_{op}/K_{max} = 0.5 + 0.1R + 0.4R^2 \tag{6}$$

$$K_{op}/K_{max} = 0.45 + 0.22R + 0.21R^2 + 0.12R^3 \tag{7}$$

The test results were processed based on the Elber's model (Eq. (6)) and the Schijve's model (Eq. (7)), as shown in Fig. 6. The crack growth rate for different stress ratios were scattered, which means the stress ratio effect was not eliminated. It was not appropriate to consider ΔK_{eff} as the fatigue crack growth control factor for high-strength steel.

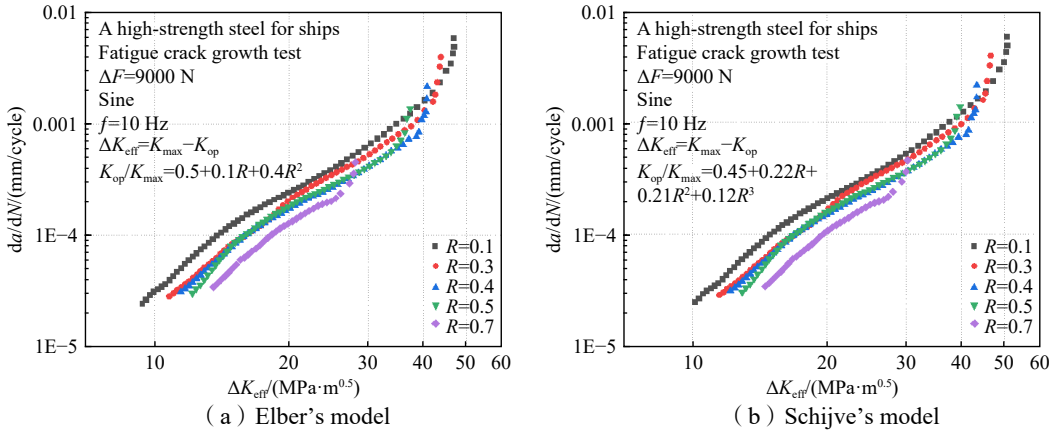

（a）Elber's model （b）Schijve's model

Fig.6 Results of crack growth rate for different crack closure models

Donald et al[18], for the fatigue behavior of aluminum alloys at stress ratios of 0.1 and 0.7, found that the fatigue crack growth rate did not depend entirely on ΔK_{eff}, but was also related to K_{max}. In addition, so far there is a lack of measurement methods that can truly reflect the crack closure parameters of metals. In view of these problems, some researchers have neglected crack closure and described the crack growth behavior by substituting the basic fracture mechanics parameters of ΔK and K_{max}. A dual-parameter-driving model was proposed[8]. This model suggested that both ΔK and K_{max} would cause crack growth for different stress ratios. When the stress ratio was low, the driving factor of crack growth was mainly K_{max}, while ΔK accounted for a higher percentage at a high stress ratio. The dual-parameter-driving model was shown in Eq. (8).

$$K^* = (K_{max})^{\lambda}(\Delta K^+)^{1-\lambda} \tag{8}$$

where K^* is a new crack growth driver, $\mathrm{MPa}\cdot\mathrm{m}^{0.5}$; λ is the material parameter that indicates the sensitivity of K^* to K_{max}, which could be obtained by fitting the experimental data; if $R \geqslant 0$, $\Delta K^+ = \Delta K$; if $R \leqslant 0$, $\Delta K^+ = K_{max}$.

Based on the dual-parameter-driving model, the fatigue crack growth rates with driving factor K^* are shown in Fig. 7. The crack growth rates test data at each stress ratio (R= 0.1, 0.3, 0.4, 0.5, 0.7) tend to overlap. This indicates that it is reasonable to use K^* as the crack growth driving factor for high-strength steel. The dual-parameter-driving model can better explain the stress ratio effect of high-strength steel during the Paris stage.

2.3 Fracture morphology

The specimens were cut for macroscopic analysis, and the fracture surface was analyzed by SEM for microscopic morphology. Fig. 8 is a diagram of the specimen before cutting. As can be seen from the figure, the fatigue crack grew forward along the width direction of the specimen. In the whole crack growth process,

the crack growth path is relatively straight, without obvious deflection, which indicates that the internal micro-structure of the material is relatively uniform.

Fig. 9 shows the macroscopic morphology of the fracture of the specimen. From the figure, it can be concluded that the specimen fracture face was gray in general. At the early stage of crack growth, the open displacement of the two crack surfaces were very small. The interaction between the surfaces made the fatigue section of high-strength steel very flat. However, as the crack length increased, the open displacement of the crack became larger and the interaction between the crack surfaces weakened. The fracture surface became rougher and rougher, and even clearly visible micro-voids appeared in the unstable fracture region.

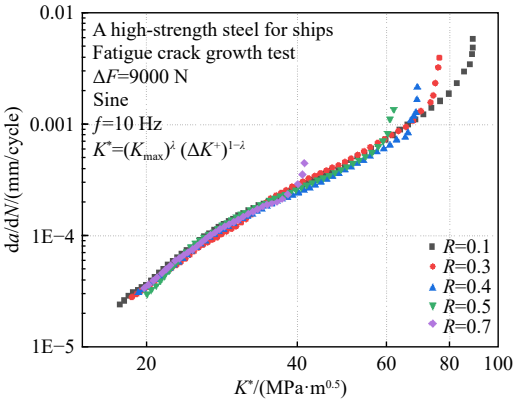

Fig.7 Results of crack growth rate based on dual-parameter-driving model

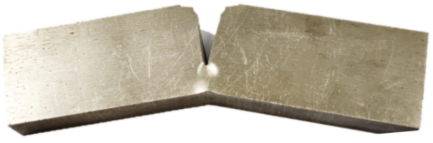

Fig.8 Fatigue crack growth specimen

Fig.9 Macroscopic appearance of the fracture

Fig. 10 shows the microscopic morphology of different stages of crack growth. In the crack initiation stage, a large number of river-like patterns as well as tiny secondary cracks appeared in the section of high-strength steel. The appearance of river-like patterns was the result of localized small plastic deformation of the section. The direction of the secondary cracks was more disorganized.

In order to further analyze the crack growth mechanism of high-strength steel, the local typical characteristic areas in the Paris stage and the destabilized growth stage were taken for high magnification microscope observation, as shown in Fig. 10(b)–(c). The fatigue characteristics of the section in Paris stage were more obvious, and a large number of fatigue glow lines appeared, whose direction was perpendicular to the crack growth direction. Compared with the crack initiation stage, the depth of secondary cracks in the Paris stage increased significantly and the section began to become uneven, which indicated that the fatigue damage was more serious in this stage.

The section in the destabilization stage of crack growth became more uneven, and a large number of spherical steel matrix debris and micro-porous pits appeared on the section in Fig. 10(c). This was due to the high stress level at this stage and non-negligible plastic deformation of the material. Under fatigue loading, strong grain slippage and dislocation buildup occurred within the high-strength steel, leading to the appearance of micro-porous pits in some places. From the viewpoint of fracture mechanism, this high-strength steel belongs to micro-hole aggregation fracture.

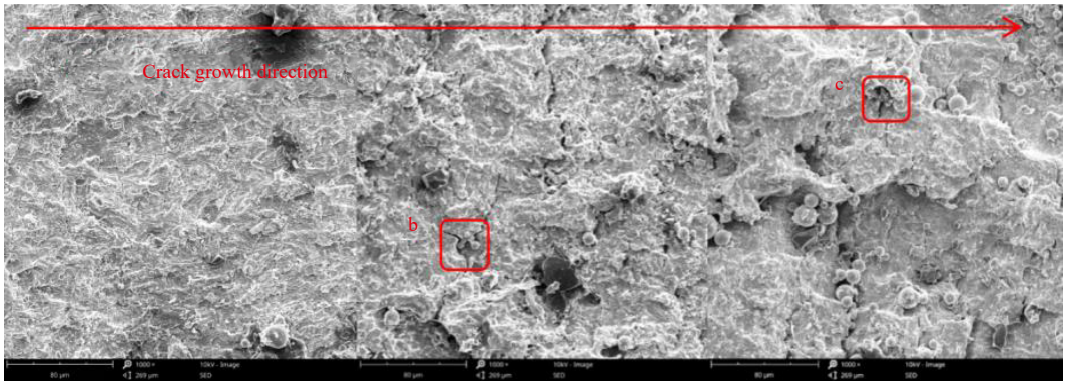

（a）Microscopic fracture morphology of different regions along the crack growth direction

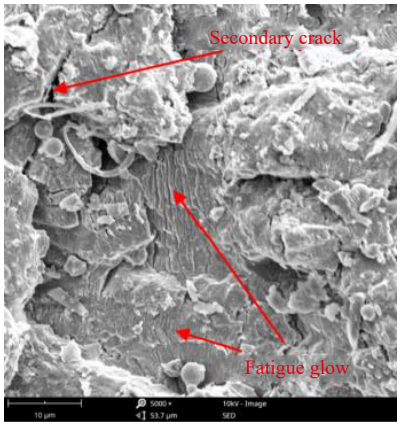

（b）Localized microscopic morphology of paris stage

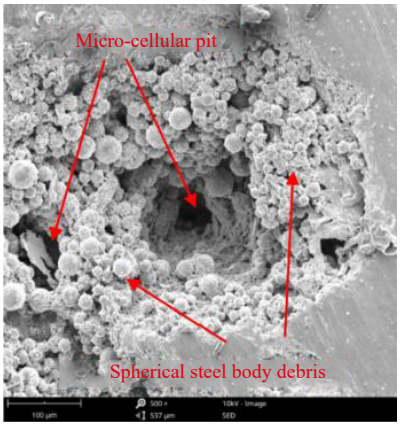

（c）Localized microscopic morphology of the destabilization stage

Fig.10 Microscopic fracture morphology of high-strength steel at different crack growth stages

3 Fatigue crack growth rate prediction

3.1 Prediction model and parameter determination

Wang et al[19] developed an improved crack growth model as shown in Eq. (9). The model can describe the three stages of crack growth and has a more ideal forecasting ability.

$$\frac{\mathrm{d}a}{\mathrm{d}N}=\frac{C\left[K_{\max}\cdot(1-f_{\mathrm{op}})-\Delta K_{\mathrm{eff-th}}\right]^{m}}{1-(K_{\max}/K_{\mathrm{C}})^{n}} \tag{9}$$

where C and m are parameters describing the slope and intercept of the crack growth rate curve in double logarithmic coordinates; $K_{\max}$ is the maximum stress intensity factor at the tip of the crack ($\mathrm{MPa}\cdot\mathrm{m}^{0.5}$), $f_{\mathrm{op}}=K_{\mathrm{op}}/K_{\max}$, is the crack opening function; $\Delta K_{\mathrm{eff-th}}$ is the range of the effective stress intensity factor at the threshold ($\mathrm{MPa}\cdot\mathrm{m}^{0.5}$), K_{C} is the fracture toughness of the material ($\mathrm{MPa}\cdot\mathrm{m}^{0.5}$), and n is the parameter describing the unstable fracture.

The improved crack growth model represents the crack closure behavior by f_{op}, which in turn describes the crack growth under different stress ratios. However, the experimental results in this paper prove that the dual-parameter-driving model can better describe the stress ratio effect of marine high-strength steels than the crack closure model. Therefore, with the combination of Eq. (9), a dual-parameter-driving crack growth prediction model was established based on the experimental results, as shown in Eq. (10).

$$\frac{\mathrm{d}a}{\mathrm{d}N}=\frac{C(K^{*}-K_{\mathrm{th}}^{*})^{m}}{1-(K_{\max}/K_{\mathrm{C}})^{n}} \tag{10}$$

where K^* is dual-parameter driving factor ($MPa \cdot m^{0.5}$), and K_{th}^* is the fatigue threshold considering a dual-parameter drive ($MPa \cdot m^{0.5}$).

The crack growth behavior in the near-threshold region is more sensitive to the stress ratios[20]. A stress ratio modification parameter $f(R)$ was introduced, as Eq. (11).

$$K_{th}^* = K_{th,max}{}^{\lambda} \cdot \Delta K_{th}{}^{1-\lambda} \cdot f(R) \tag{11}$$

$$f(R) = 1 + \alpha R + \beta R^2 \tag{12}$$

where ΔK_{th} denotes the long crack growth threshold ($MPa \cdot m^{0.5}$), $K_{th,max}$ denotes the maximum stress intensity factor corresponding to the threshold ($MPa \cdot m^{0.5}$), K_{th}^* is the fatigue threshold considering a dual-parameter drive ($MPa \cdot m^{0.5}$), α and β are parameters related to the stress ratio.

The relationship between the stress ratio and the fatigue threshold value K_{th}^*, before and after modification, is shown in Fig. 11. It can be seen that K_{th}^* of high-strength steel before modification decreased with the increase of stress ratio, while the trend was basically the same after modification. This indicates that the introduction of $f(R)$ well eliminated the stress ratio effect in the near-threshold stage.

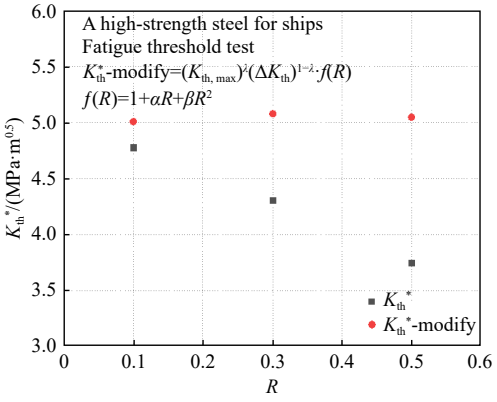

Fig.11 Original and modified fatigue thresholds K_{th}^* versus stress ratio R

Based on the dual-parameter-driving modified model, Eq. (10), the crack growth rates of high-strength steel were predicted at different stress ratios. The values of each parameter in the model are shown in Tab. 1.

Tab.1 Model parameters of Eq. (10) for high-strength steel crack prediction

R	C/(MPa$^{-m}\cdot$m$^{1-m/2}$)	m	n	λ	K_C/(MPa·m$^{0.5}$)	α	β
0.1,0.3,0.4,0.5,0.7	1.59×10^{-10}	2.05	6	0.212	107.1	0.409	0.544

3.2 Prediction results and discussion

The comparison between the predicted and experimental results of fatigue crack growth rates of high-strength steel are shown in Fig. 12. Five stress ratios were considered, which were 0.1, 0.3, 0.4, 0.5 and 0.7. As can be seen from Fig. 12(a)–(e), the results of the fatigue crack growth rate predicted by Eq. (10) were in

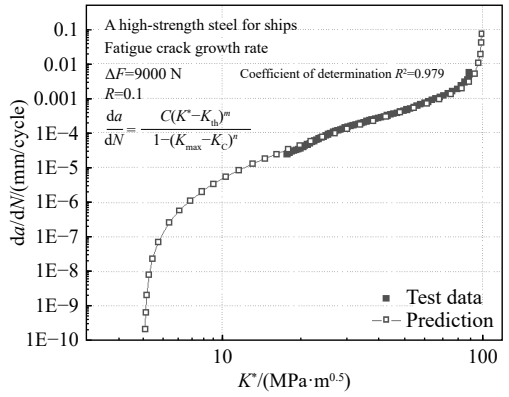

（a）R=0.1

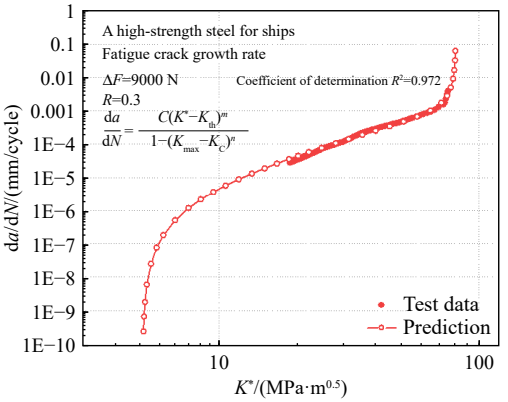

（b）R=0.3

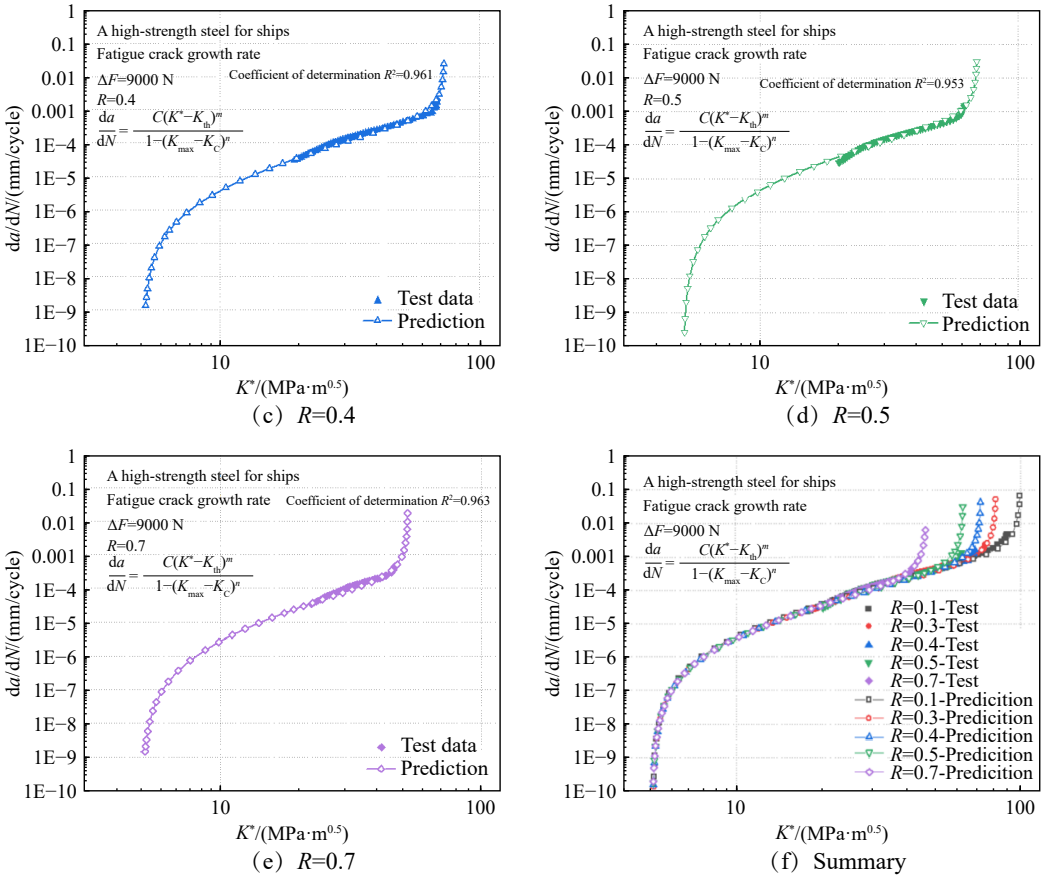

Fig.12 Comparison of fatigue crack growth rate between predicted and experimental results

good agreement with the experimental results. Between the predicted results and the test results, the coefficients of determination were 0.979, 0.972, 0.961, 0.953, and 0.953 for stress ratios of 0.1, 0.3, 0.4, 0.5, and 0.7, respectively.

From Fig. 12(f), the fatigue thresholds of this steel at five stress ratios converge to the same value $K_{\mathrm{th}}^{*}=5.03\ \mathrm{MPa}\cdot\mathrm{m}^{0.5}$. In the near-threshold and Paris region, the modified model eliminated the effect of stress ratio, and the crack growth rate curves ($\mathrm{d}a/\mathrm{d}N-K^{*}$) were consistent for different stress ratios. These curves separated only in the unstable phase. This was because the fracture of the specimen was controlled by $K_{\max}$ and K_{C}. The larger R was, the larger ΔK was, and the sooner the specimen would fracture. In conclusion, the modified model Eq. (10) has a strong prediction ability for the near-threshold stage, Paris stage and unstable stage of crack growth on high-strength steel.

To validate the prediction ability of Eq. (10) for other materials and demonstrate the advantages of the model, the fatigue crack growth behavior of titanium alloys in the literature[21] was predicted by both the improved crack growth model (Eq. (9)) and the dual-parameter-driving crack growth prediction model (Eq. (10)), and the prediction results were compared with the tests as shown in Fig. 13. For the experimental results, the crack growth rate curves of the Paris stage at different R basically overlap when K^{*} is the driving force. On the other hand, Eq. (10) described the crack growth behavior of titanium alloys more accurately and eliminated the stress ratio effect of the near-threshold stage and the Paris stage perfectly. This proved that the dual-parameter- driving crack growth prediction model developed in this paper can be applied to a wide range of materials and has a more desirable prediction capability.

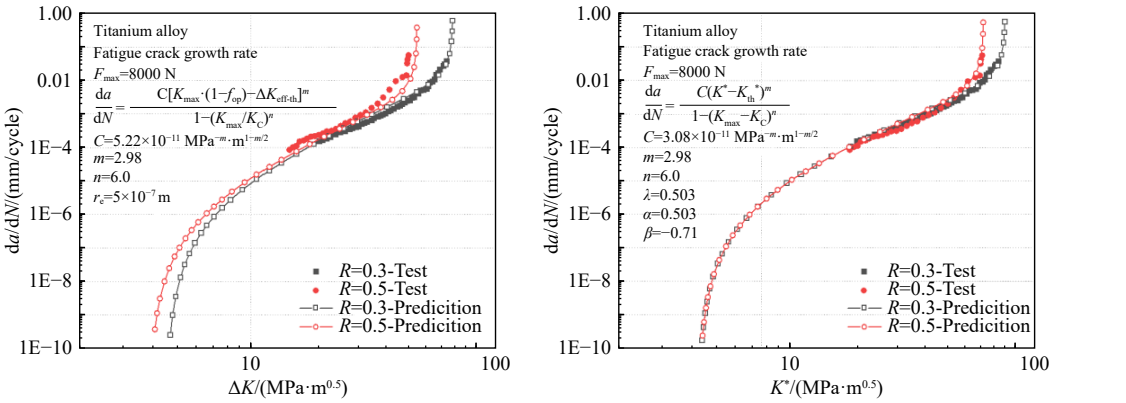

（a）Improved crack growth model　（b）Dual-parameter-driving crack growth prediction model

Fig.13 Comparison of the fatigue crack growth prediction results with experimental ones for titanium alloys[21]

4 Conclusions

In this paper, the fatigue performance of a high-strength steel for ships was investigated. Firstly, the fatigue threshold test of this steel was conducted under three stress ratios of 0.1, 0.3 and 0.5. The basic mechanical parameters were obtained. Secondly, the fatigue crack growth rate test of this high-strength steel was conducted under different stress ratios. The stress ratio effect was analyzed based on crack closure and driving force. The fracture characteristics of high-strength steel were obtained by SEM. Finally, the dual-parameter-driving model was modified based on the fatigue properties of the metal in the near-threshold stage and unstable stage. The fatigue crack growth behavior of high-strength steel was predicted using the modified model. The feasibility of the modified model was verified by comparing the prediction with the experimental results. The following conclusions were obtained.

(1) The fatigue crack growth behavior of high-strength steel has an obvious stress ratio effect. The ship steel exhibited the phenomenon that the increase of stress ratio can promote fatigue crack growth rates and lead to a decrease in fatigue life. The test data were processed by the crack closure model and the dual-parameter-driving model, and it was found that the dual-parameter-driving model could better explain the stress ratio effect of high-strength steel.

(2) A large number of secondary cracks, fatigue glow and river-like striations appeared in the fatigue section of high-strength steel. The fatigue glow was basically perpendicular to the crack growth direction. With crack growth, the section gradually became rough and the depth of secondary cracks increased. Clear micro-pores appeared in the section at the destabilized fracture stage. According to the fracture mechanism, the damage of high-strength steel belongs to micro-cavity aggregation fracture.

(3) The fatigue thresholds predicted by the modified dual-parameter-driving model were essentially the same for different stress ratios. The crack growth rate curves separated only in the unstable phase, which indicated that the fatigue stress ratio effect was eliminated by the modified model. Determination coefficients of the crack growth rates between the predicted results and the corresponding test results were all greater than 0.95. The modified model has a strong prediction ability for the fatigue crack growth behavior of high-strength steel under different stress ratios. The prediction results of titanium alloy crack growth behavior show that the modified model can be applied to various metallic materials with high accuracy.

References

[1] Zhai Y, Guo X B, et al. Analysis of fatigue fracture behavior of low-alloy high-strength steels with different strength grades[J]. Journal of Plasticity Engineering, 2023, 30(7): 145–150. (in Chinese)

[2] Riahi H, Bressolette P, et al. Random fatigue crack growth in mixed mode by stochastic collocation method[J]. Engineering Fracture Mechanics, 2010, 77(16): 3292–3309.

[3] Liu D, Liu J, et al. Corrosion fatigue crack propagation performance of DH36 steel in simulated service conditions for offshore engineering structures[J]. Journal of Chinese Society Corrosion and Protection, 2022, 42(6): 959–965. (in Chinese)

[4] Wang K, Wu L, et al. Experimental study on low temperature fatigue performance of polar icebreaking ship steel[J]. Ocean Engineering, 2020, 216: 107789.

[5] Zhong Y, Shao Y B, et al. Effect of stress ratio on fatigue crack growth rate of EH36 steel in the marine corrosive environment[J]. Materials Reports, 2023, 37(19): 192–198. (in Chinese)

[6] Wang Q. Fatigue crack growth behavior of 10Ni5CrMoV high-strength steelwelded joints[D]. Harbin: Harbin Institute of Technology, 2019. (in Chinese)

[7] Kujawski D. A fatigue crack driving force parameter with load ratio effects[J]. International Journal of Fatigue, 2001, 23(S1): 239–246.

[8] Martelo D, Mateo A, et al. Fatigue crack growth of a metastable austenitic stainless steel[J]. International Journal of Fatigue, 2015, 80: 406–416.

[9] Wei H T. Fatigue crack growth behavior of SA508Gr. 3Cl. 2 under different stress ratios and effect of fatigue damage on fracture toughness[D]. Hangzhou: Zhejiang University of Technology, 2020. (in Chinese)

[10] Wang K, Sun Z Y, et al. Prediction method of dwell-fatigue crack growth behavior of new titanium alloy[J]. Journal of Ship Mechanics, 2023, 27(6): 877–887.

[11] Wang K, Wu L, et al. Study on the overload and dwell-fatigue property of titanium alloy in manned deep submersible[J]. China Ocean Engineering, 2020, 34(5): 738–745.

[12] Li Y Z, Xie X B, et al. Prediction method of the dwell-fatigue crack growth for titanium alloys and its validation on IMI834 at room temperature[J]. Journal of Ship Mechanics, 2019, 23(3): 317–331.

[13] Wu L, Bian C, et al. A simplified prediction model of dwell-fatigue crack growth behaviour for titanium alloy[J]. Ships and Offshore Structures, 2022, 17(11): 2408–2415.

[14] GB/T 6398-2017, Technical Committee 183 on Steel of Standardization Administration of China. Metallic materials. Fatigue testing. Fatigue crack growth method[S]. Beijing: Beijing Standard Press, 2017.

[15] Elber W. Fatigue crack closure under cyclic tension[J]. Engineering Fracture Mechanics, 1970, 2(1): 37–45.

[16] Elber W. The significance of fatigue crack closure[J]. AstmStp, 1971, 486: 230–242.

[17] Schijve J. Some formulas for the crack opening stress level[J]. Engineering Fracture Mechanics, 1980, 14(3): 461–465.

[18] Donald K, Paris P C. An evaluation of ΔK_{eff} estimation procedures on 6061-T6 and 2024-T3 aluminum alloys[J]. International Journal of Fatigue, 1999, 21(S1): S47–S57.

[19] Wang F, Chen F L, et al. Applicability of the improved crack growth rate model and its parameters estimation method[J]. Journal of Ship Mechanics, 2010, 14(3): 252–262.

[20] Larissa D, Arthur J S, et al. Recent developments in the determination of fatigue crack propagation thresholds[J]. International Journal of Fatigue, 2022, 164: 107131.

[21] Bian C C. Research on fatigue life assessment method of titanium alloy welded parts based on crack propansion[D]. Zhenjiang: Jiangsu University of Science and Technology, 2021. (in Chinese)

船用高强钢疲劳裂纹扩展行为研究

雷银慧[1], 王　珂[1], 张若楠[2,3], 李永正[1], 秦　闯[1], 韦朋余[2,3]

（1. 江苏科技大学 船舶与海洋工程学院, 江苏 镇江 212003; 2. 中国船舶科学研究中心, 江苏 无锡 214082; 3. 深海技术科学太湖实验室, 江苏 无锡 214082）

摘要: 船用高强钢作为一种典型的钢材, 其疲劳问题一直受到学者们的重视。本文采用试验方法研究某船用高强钢的疲劳性能和裂纹扩展机理, 首先开展不同应力比下高强钢的疲劳门槛值试验和疲劳裂纹扩展速率试验, 分析应力比对船用钢疲劳特性的影响规律; 其次, 利用扫描电子显微镜分析高强钢裂纹扩展试样断面, 揭示高强钢裂纹扩展及失效机理; 最后, 基于上述研究结果, 从裂纹闭合和驱动力两个角度分析高强钢的应力比效应, 并且考虑近门槛值阶段和失稳阶段的疲劳行为, 建立船用高强钢疲劳裂纹扩展行为预报模型, 通过试验数据验证模型的准确性。此外, 通过与文献数据及现有模型的对比, 验证修正模型对多种材料的适用性和出色的预测能力。

关键词: 高强钢; 疲劳试验; 载荷比效应; 双参数驱动力; 预测模型

中图分类号: TG111.8　　**文献标识码:** A

基金项目: 国家自然科学基金资助项目(52071161); 国家重点研发计划项目(2022YFB3404800)

作者简介: 雷银慧(1999–), 女, 硕士研究生;

王　珂(1979–), 女, 江苏科技大学教授;

张若楠(1995–), 男, 中国船舶科学研究中心工程师;

李永正(1980–), 男, 江苏科技大学教授;

秦　闯(1993–), 男, 江苏科技大学助理实验师;

韦朋余(1982–), 男, 中国船舶科学研究中心研究员。